BJRS
BRAZILIAN JOURNAL OF RADIATION SCIENCES

doi.org/10.15392/2319-0612.2025.2843
2025, 13(2A) | 01-20 | e2843
Submitted: 2025-01-28
Accepted: 2025-05-07

Reference Male Phantom for Internal Dosimetry-RMPID: Physical model in 3D-printing for whole-body counter calibration

Sales [a*], H. ; Andrade [a], E.M.R. ; Mendes [a], B.M.

[a] Centro de Desenvolvimento da Tecnologia Nuclear, CDTN, Av. Presidente Antônio Carlos, 6627, Pampulha, CEP: 31270-901 Belo Horizonte, MG, Brazil.

*Correspondence: hirys.sales@cdtn.br

Abstract: *In vivo* internal dosimetry can use a whole-body counter (WBC) to estimate radionuclides' incorporated activity (Bq) in internally contaminated individuals. The WBC must be calibrated to convert the count rate from the detector into activity incorporated in the person. Active physical phantoms could be used for the calibration procedure. Additive manufacturing allows the physical reproduction of ICRP computational models with good geometric fidelity. This study aims to develop imaging manipulation techniques to generate stereolithography (STL) parts for the 3D printing a male physical phantom based on the Adult Male Reference Computational Phantom (RCP_AM) model provided in the ICRP 110 publication. The Reference Male Phantom for Internal Dosimetry (RMPID) was developed based on the model provided by the ICRP in text file format containing the RCP_AM segmentation information. It was processed with an in-house C++ program that generated images in RAW format (Unprocessed images). The images were manipulated using freeware: ImageJ, MeshLab, FreeCAD, and Meshmixer. A set of 22 hollow portions, 44 pieces including the lids, which fit together, were obtained. The RMPID was printed in PLA (Polylactic Acid) on the Creality Ender 5 Plus 3D printer. The 3D-printed phantom parts passed leak tests, proving that imaging manipulation techniques resulted in well-sealed parts. That will allow the phantom to be safely filled with tissue-equivalent material containing a calibrated activity of the selected radionuclide. The design also makes the simulator easier to handle and to assemble during calibration routines.

Keywords: Internal Dosimetry; Anthropomorphic Phantom; 3D Print; Whole-body Counter.

SBPR

BJRS
BRAZILIAN JOURNAL OF RADIATION SCIENCES

doi.org/10.15392/2319-0612.2025.2843
2025, 13(2A) | 01-20 | e2843
Submitted: 2025-01-28
Accepted: 2025-05-07

Fantoma de Referência Masculino para Dosimetria Interna-RMPID: modelo físico em impressão 3D para calibração de contador de corpo inteiro

Resumo: A dosimetria interna in vivo pode usar um contador de corpo inteiro (WBC) para estimar a atividade incorporada (Bq) de radionuclídeos em indivíduos internamente contaminados. O WBC deve ser calibrado para converter a taxa de contagem do detector em atividade incorporada na pessoa. Fantomas físicos ativos podem ser usados para o procedimento de calibração. A manufatura aditiva permite a reprodução física de modelos computacionais do ICRP com boa fidelidade geométrica. Este estudo visa desenvolver técnicas de manipulação de imagens para gerar peças de estereolitografia (STL) para a impressão 3D de um fantoma físico masculino baseado no Fantoma Computacional de Referência do Adulto Masculino (RCP_AM) fornecido na publicação ICRP 110. O *Reference Male Phantom for Internal Dosimetry* (RMPID) foi desenvolvido com base no modelo fornecido pelo ICRP em formato de arquivo de texto contendo as informações de segmentação do RCP_AM. Ele foi processado com um programa C^{++} que gerou imagens em formato RAW. As imagens foram manipuladas usando freewares: ImageJ, MeshLab, FreeCAD e Meshmixer. Foi obtido um conjunto de 22 porções ocas, 44 peças incluindo as tampas, que se encaixavam. O RMPID foi impresso em PLA (ácido polilático) na impressora 3D Creality Ender 5 Plus. As peças do simulador impressas em 3D passaram nos testes de estanqueidade, comprovando que as técnicas de manipulação de imagens resultaram em peças bem seladas. Isso permitirá que o simulador seja preenchido com segurança com material equivalente ao tecido, contendo uma atividade calibrada do radionuclídeo selecionado. O design também facilita o manuseio e a montagem do simulador durante as rotinas de calibração.

Palavras-chave: Dosimetria interna; Fantoma antropomórfico; Impressão 3D; Contador de corpo inteiro.

SBPR

1. INTRODUCTION

Internal dosimetry combines tools and procedures to calculate the time-integrated effective dose after the internal incorporation of radionuclides into an individual. It can be applied to medical exposures (such as nuclear medicine), occupational exposures, and public exposures (in case of radiological or nuclear accidents) [1], [2]. Occupationally, radionuclides can be incorporated through several routes. The most significant are inhalation and ingestion. Skin absorption or injury uptake are alternative routes [3], [4]. In vivo or in vitro bioassay methods are used to quantify the incorporated activity, and the contamination scenario will be taken in to consideration in these evaluations[2], [3], [5].

The in vitro method involves the determination of the activity concentrations of radioactive materials in excreta (urine, feces) or other biological materials [6], [7]. The in vivo method often uses whole-body counters (WBC) to evaluate the count rate (CPS) detected from the monitored individual emissions. The WBC detector is typically NaI(Tl) (thallium-activated sodium iodide) or HPGe (hyper pure germanium). The count rate should be converted into incorporated activity during monitoring based on the system's calibration coefficient [3], [6], [8]. **Figure 1** depicts the WBC of the internal dosimetry laboratory of the Nuclear Technology Development Center (LDI/CDTN). The system comprises an 8"x4" NaI(Tl) detector and a shadow-shielded bed to reduce environmental background radiation's impact on the detection system. Geometries different from WBC can be used to evaluate specific organs, such as the lungs, liver, and thyroid.

Precise calibration of the in vivo system is essential to avoid uncertainties propagating into the committed effective dose calculation [8]. The calibration procedure generally uses anthropomorphic and anthropometric physical phantoms, such as the ones presented in the ICRU report 48 [9], as active models for calibration. Such models are based on solid

structures homogeneously filled with a known activity of a given radionuclide [8], [9], [10]. Alternatively, in vivo systems can be calibrated using computer simulators, mathematical models, and Monte Carlo methods.

Figure 1: LDI/CDTN whole-body counter.

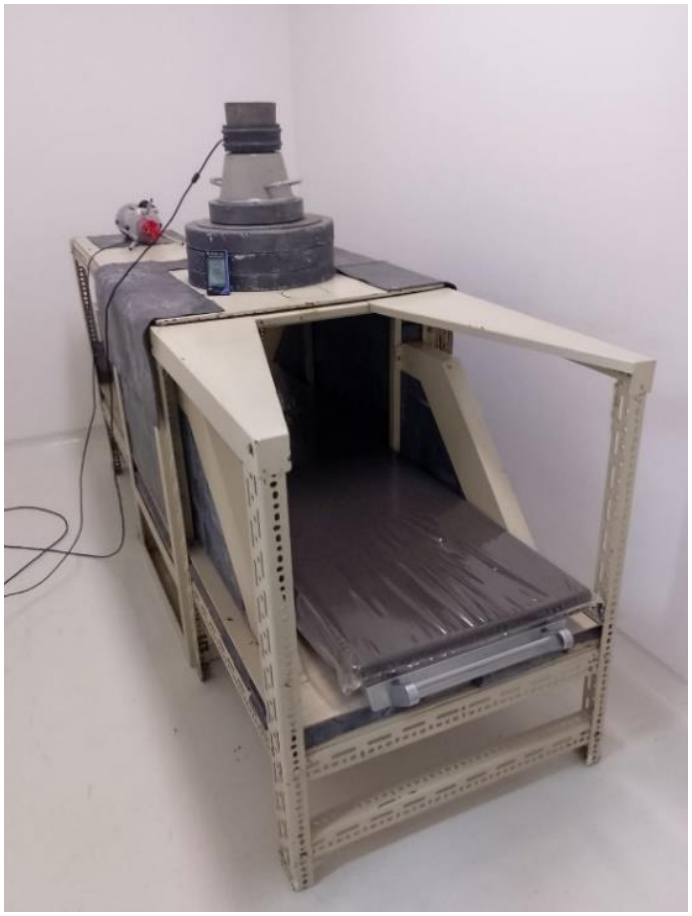

Source: Author's collection

The efficiency calibration of the WBC consists of determining the relationship between photon emission rates of a radioactive phantom and the count rate registered on the detector for specific energy photopeaks [11]. It is also possible to obtain energy-dependent calibration factors relating the measured count rate of a photopeak to the radionuclide activity in the simulator [8]. **Figure 2** illustrates a typical efficiency calibration curve for the NaI(Tl) detector.

Figure 2: Efficiency versus Energy graph obtained for the LDI Whole-Body Counter (WBC), using the physical phantom, PET BOMAB, containing known activities of Co-60, Ba-133, and Cs-137.

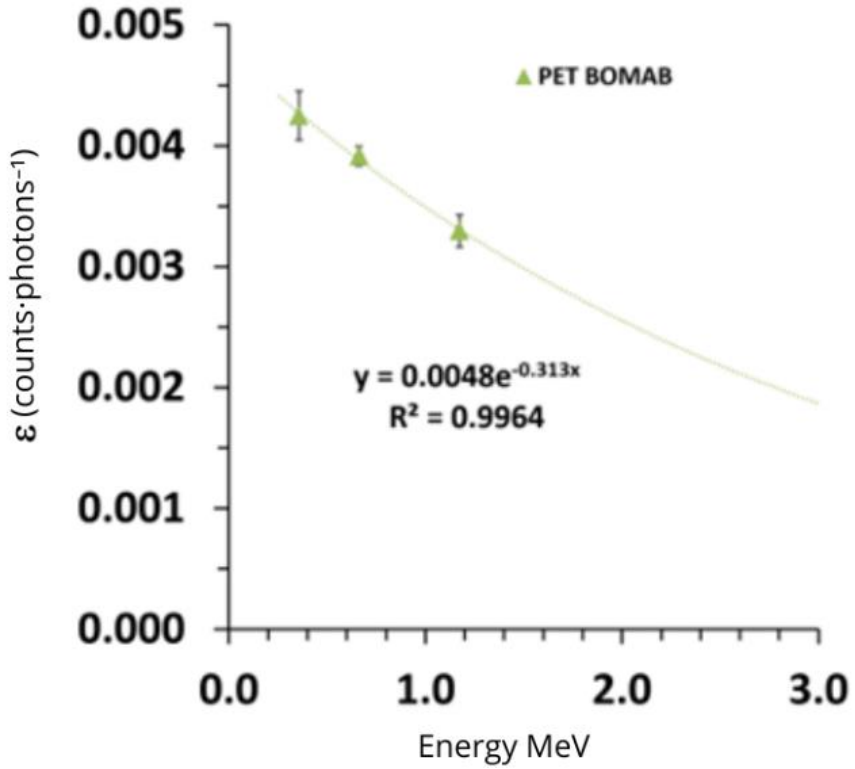

Source: Author's collection

Since the calibration coefficient (CC) is an essential parameter for determining the incorporated activity and, consequently, the committed effective dose, it is necessary to study methodologies to reduce the uncertainties associated with the CC obtained for in vivo monitoring systems. In vivo monitoring uncertainties are categorized into Type A statistical nature, related to counting statistics, and Type B errors associated with counting geometry, positioning of the individual/simulator, and differences between the phantom and the individual, including geometric features [2], [8], [12], [13]. Physical phantoms available on the market, such as the BOMAB (BOttle Mannikin ABsorber Phantom) [14] or family phantoms "Emma" [15], have simplified geometric shapes designed to approximate human geometry. However, this configuration introduces Type B uncertainties into the system [16].

The additive manufacturing (AM) allows the creation of anthropomorphic simulators that can replicate complex geometries, overcoming the limitations of the geometrical shape phantoms. These simulators are being developed for various applications, including quality control of radiological equipment and dose distribution calculation in radiotherapy. [17], [18].

Physical phantoms based on additive manufacturing are being developed to calibrate internal dosimetry in vivo monitoring systems. Among these models, a physical thyroid phantom was developed by Moratelli (2021) for the calibration of in vivo monitoring systems designed to evaluate I-131 incorporations. The phantom features anatomical realism and is based on the female voxelized thyroid model of ICRP 110 (2009) [19]. Additionally, the liver phantom was developed using 3D printing by Tran-Gia (2016) [20] for calibration in SPECT and in vivo monitoring of occupationally exposed workers (OEW). Furthermore, the 3D lung model developed by Capello (2024) is designed for calibration and performance testing of pulmonary counting systems in Canada [21].

Previously, the research group at the LDI-CDTN (Internal Dosimetry Laboratory of the Nuclear Technology Development Center) developed the Reference Female Phantom for Internal Dosimetry (RFPID) illustrated in **Figure 3**, part of the series of voxelized phantoms from ICRP 110, based on the ICRP-110 Adult Female Computational Reference Phantom (RCP_AF) [10], [22]. The RFPID is a hollow structure 3D-printed using Polylactic Acid (PLA) filament, designed as a whole-body phantom to calibrate the in vivo system at LDI-CDTN [10]. The printed RFPID model was divided into 16 parts with lids (**Figure 3 b and c**), allowing for the filling and sealing of the structure. However, it presents design limitations that hinder its handling, requiring shrink-wrap plastic to position the simulator components properly [10].

Figure 3: A) Whole-body phantom Reference Female Phantom for Internal Dosimetry (RFPID). B-C) Parts with lids.

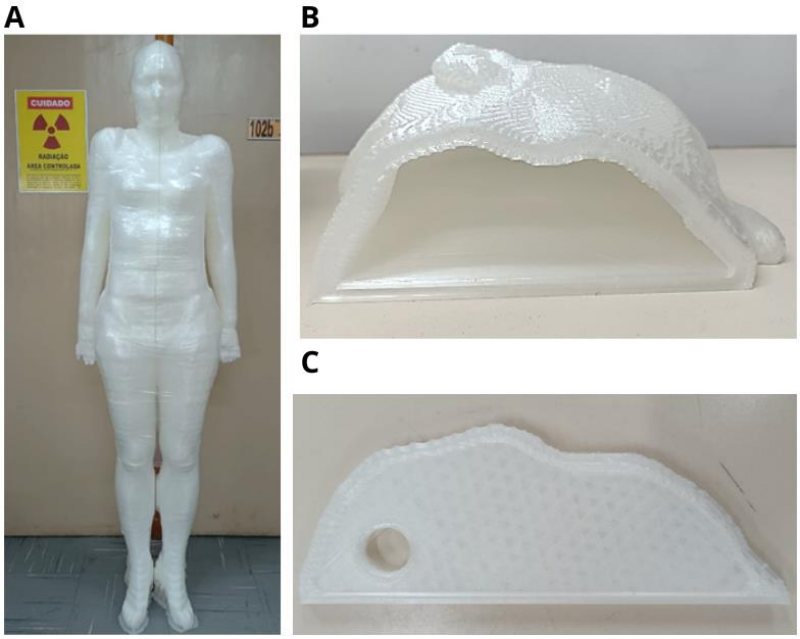

Source: Adapted from [10]

To improve the AM production of physical phantoms initiated in our group with the development of RFPID, this study aims to develop new image manipulation techniques and further refine the simulator's geometry, now utilizing the ICRP Adult Male Reference Computational Phantom (RCP_AM) [22]. The simulator developed in this research will be called Reference Male Phantom for Internal Dosimetry (RMPID).

1.1 Male reference voxel phantom from ICRP 110.

The model selected for this study was the Adult Male Reference Computational Phantom (RCP_AM), defined by ICRP-110 [22]. The male computer phantom was produced from a set of whole-body clinical computed tomography images of a 38-year-old man 176 cm in height and 70 kg in weight. The computational model has the same height, and the weight was reduced to 73 kg to match the reference man's weight [23]. The RCP_AM computational phantom was segmented into distinct organs and tissues with their corresponding densities and elemental compositions, as illustrated in **Figure 4**. Nevertheless, this study focuses only on the external shape of the model [22].

Figure 4: The front view of the ICRP-AM is a voxel model representing the ICRP adult reference male.

Source: Adapted from [24]

During the CT scan, the reference man was positioned supine, with his arms parallel to his body. The data set consisted of 220 256x256 pixel slices. The original voxel size was 8 mm high, with an in-plane resolution of 2.08 mm, resulting in a voxel volume of 34.6 mm^3. Table 1 describes the main physical characteristics of the AM [22].

Table 1: Characteristics of the RCP_AM/ICRP Phantom.

Characteristic	Male Phantom
Height (m))	1.76
Mass (kg)	73.0
Number of tissue voxels	1.946.375
Slice thickness (voxel height, mm)	8.0
In-plane voxel resolution (mm)	2.137
Voxel volume (mm^3)	36.54
Number of columns	254
Number of rows	127
Number of slices	220 (+2)*

*Additional slices of skin at the top and bottom.

Source: adapted from [22]

2. MATERIALS AND METHODS

The ICRP provides the reference male phantom in text format (RCP_AM) with the DAT extension [22]. This ASCII file contains a set of tissue codes representing all segmented organs of RCP_AM. The initial step was transforming the RCP_AM ASCII file into a three-dimensional image using an in-house C^{++} program. It processes the ASCII file and generates a three-dimensional voxel matrix, with each voxel "filled" with the corresponding tissue code. To perform this task, the code uses the CImg library, which is used to create and manipulate RAW-type images.

The RAW axial image sequence was extracted and binarized using the ImageJ® software [25]. Thus, the heterogeneous tissue structures of the computational phantom were converted into a uniform solid piece, preserving the phantom's original external shape and geometry. To enhance the visual quality of the simulator for 3D printing, the Smooth Laplacian filter was utilized in the MeshLab software [26] to mitigate the pixelated appearance of the model. The result of this process is illustrated in **Figure 5.**

Figure 5: ICRP-110 reference male phantom after the binarization process and geometry surface smoothing

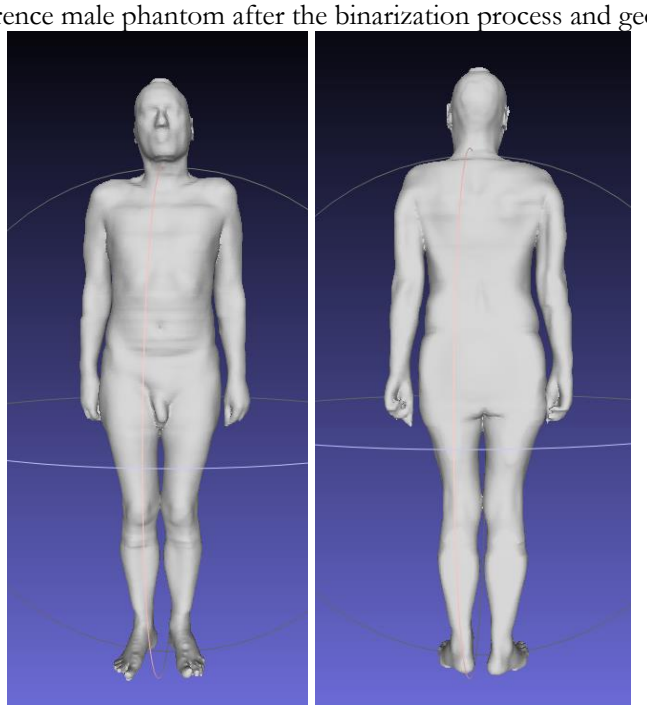

Source: Author's collection.

The binarized images (solid and homogeneous) were imported into the FreeCAD software. [27]. At this stage, the simulator was divided into two sides (right and left). Later, each side was split into 20 cm high portions to fit the 3D printer's printable volume (**Figure 6 a**). These portions were manipulated on the FreeCAD to create fittings similar to puzzle pieces. These fittings were positioned between the divisions of the pieces, both in horizontal and vertical lines, as shown in **Figure 6 a**. The fittings sizes varied, with 8 mm diameter designated for smaller areas, such as the hands, and 10 mm diameter for larger parts, such as the chest. The design of the fittings was transformed into a solid body, which permitted their extraction from the geometry of the phantom, thereby forming 22 discrete objects. **Figure 6 a, b and c** illustrate the process of separating and creating the individual parts, which allows them to be adapted to the size of the printing volume of the 3D printer used.

Figure 6: A-B) Division of the RCP_AM 3D image using FreeCAD software. Division in Right and Left sides, and the obtention of 22 parts with puzzle-like fittings. C) Separated right head portion. D) Division of the part right head part into a lid and a hollow part. E) Hollow piece of the right head part. F) Lid of the right head hollow part, note the presence of the puzzle-like fitting.

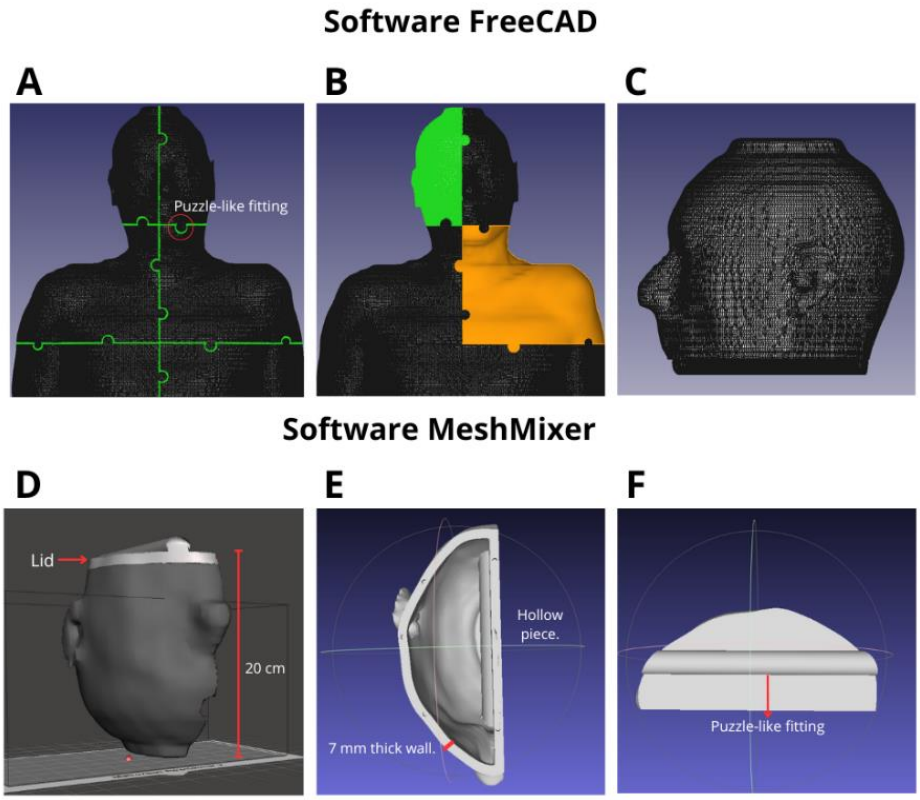

Source: Author's collection.

All the phantom parts will be filled with equivalent tissue material containing a calibrated radionuclide activity. Thus, the parts must have a hollow interior. Once the fittings have been created, it is necessary to export the parts separately to facilitate individual manipulation in the Meshmixer software [28]. As illustrated in **Figure 6 d**, the hollow function was applied at this stage, thus transforming the solid part into a hollow portion with a wall thickness of 7 mm. Subsequently, the hollow portion was divided into two distinct components: a lid and a hollow part, as illustrated in **Figure 6 e and f**. It is important to note that all 22 parts underwent the same process, creating a lid and a hollow portion.

Two potential methods were tested to produce the fitting between the lid and the hollow part. In the first, using FreeCAD software, pins were designed and then attached to the edge of the lid. The geometry of the pins was then subtracted from the 7 mm wall of the hollow part to create the recess. **Figure 7** shows the result of this process. The scale of the pins attached to the lid was adjusted to ensure a proper fit. The part was then printed at full scale to evaluate the fit. In the second method, the geometry of the lid was redrawn, generating a raised area 5 mm away from the external edge of the lid. As shown in **Figure 8 a**, in the Meshmixer software, the edge of the lid was cut off, producing a Slice that was separated from the rest of the geometry. In FreeCAD software, the Slice was resized, equalizing the XYZ axes with 1 mm, thus allowing the structure to be scaled down, resulting in a piece smaller than the external edge of the lid. The next step was to position the Slice centrally (**Figure 8 a**) on the lid and apply the union of the two geometries. The result is shown in **Figure 8 b**. Still, in the FreeCAD software, the new lid geometry must be subtracted from the structure of the hollow part; this will form a 7 mm wall recess, as shown in **Figures 8 c and d**. The 5 mm edge was altered by reducing 0.2 mm on the X-Y axes and attached to the lid. This reduction process was necessary so that the structure could fit appropriately into the space created in the hollow part by subtracting the previous scale.

Figure 7: . The first method of pins fitting in the lid and in the hollow part. A) Pins positioned in the lid B) Subtraction of the pins in the 7 mm wall of the hollow part.

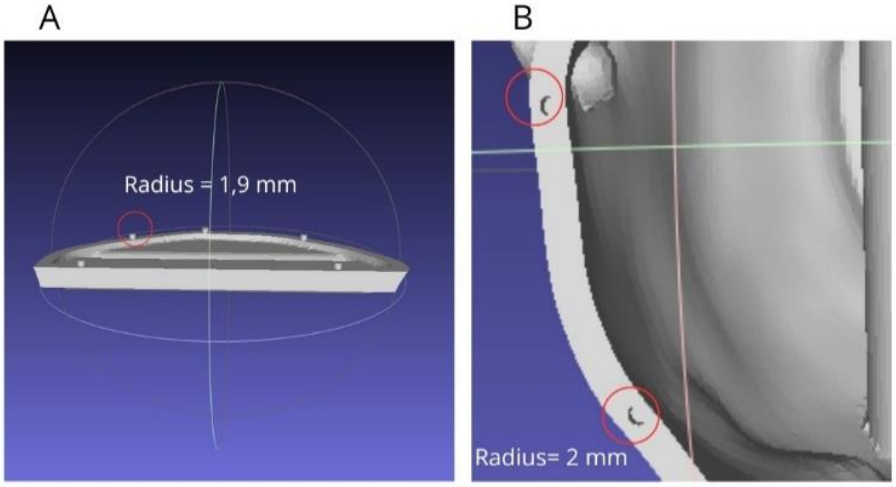

Source: Author's collection.

Figure 8: Creating the step-shaped fitting in the lid and the hollow part. A) Slice taken from the geometry of the lid and positioned with new scale. B) Final product lid with 5 mm protrusion. C-D) Result of subtracting the 5 mm fitting from the 7 mm wall of the hollow piece.

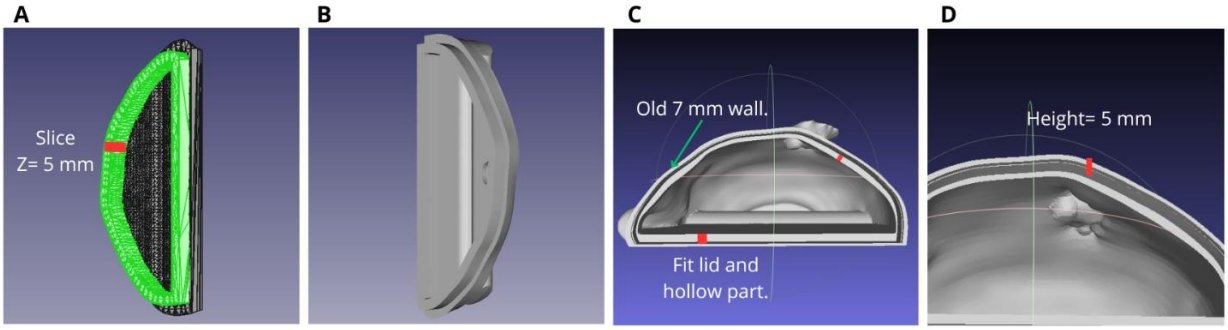

Source: Author's collection.

Mechanisms have been implemented to mitigate the risk of spillage and leakage when filling the parts with radioactive tissue-equivalent material. The main lid of the hollow portions was given a hole and a secondary lid to seal the part without excess air after filling. The hole was created using FreeCAD software, where two cylinders were generated, with 10 mm and 8 mm radius for most of the primary lids. However, due to the different shapes and sizes of the primary lids, some parts received holes with smaller dimensions to adapt to the available space (**Figure 9**). The cylinders were joined to form a single solid, then positioned and subtracted from the primary lid.

Figure 9: Illustration of the methodology for creating the aperture in the lid. A) The dimensions and position of the mold for the hole. B) Lid with hole. C) Lid reduced to fit the hole.

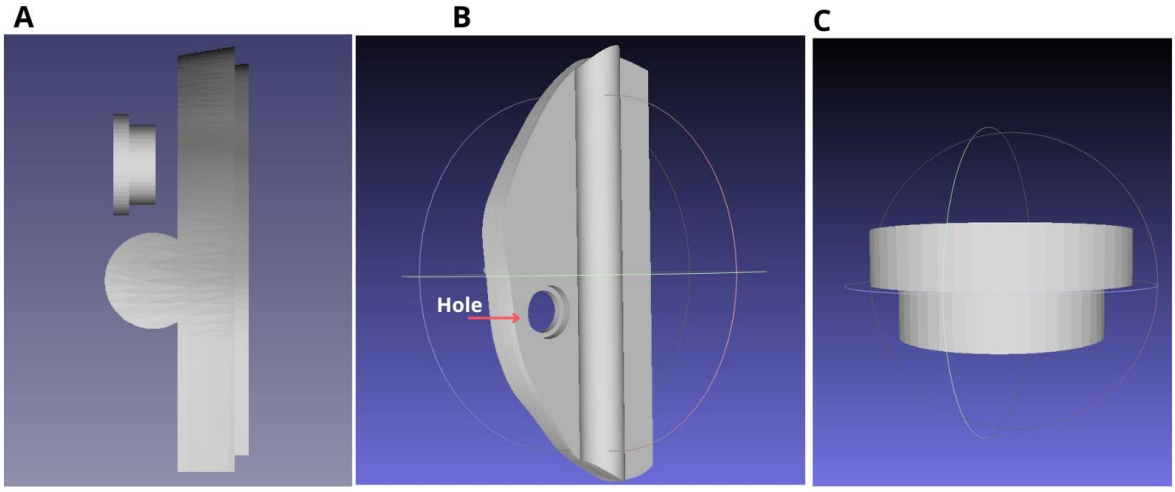

Source : Author's collection.

The parts were printed on two Creality Ender 5 Plus 3D printers manufactured by Shenzhen Creality 3D Technology CO., LTD, in China. These printers use filament deposition fusion (FDM) technology with a printable volume of 35x35x40 cm^3. PLA (polylactic acid) filament was used for printing due to its attenuation characteristics, which are similar to soft tissue, and because it is a material that is easy to handle in open 3D printers [10], [29]. The parts were sliced using the Creality Slicer software. The printing parameters were the same as those used to develop the RFPID [10].

2.1. Application of epoxy resin and leak test.

The printed parts were painted with epoxy resin (Real Epóxi) to avoid leakage of the tissue-equivalent material containing the radioactive material. Three layers of resin mixed with green pigment were applied inside all the hollow pieces and the respective lids. The pigment will serve as a marker to identify the resin-filled areas. Acetic silicone glue (Tekbond - Saint-Gobain) was used to bind and seal the lids and the hollow parts. After applying the three layers of epoxy resin, a leakage test was applied to observe possible infiltrations and leaks in the parts.

3. RESULTS AND DISCUSSIONS

The puzzle-like fitting was tested on a miniature version (**Figure 10 a**) and demonstrated improvement in handling of the pieces and a more precise alignment between the structures when compared with RFPID [9]. However, the full-scale printed components (**Figure 10 b**) did not achieve the intended goal of securely attaching one piece to another, indicating the need to fine-tune the fitting elements' alignment to ensure proper locking. The pieces were then reprinted with the adjusted positioning of the fittings, resulting in an effective locking mechanism, even after applying three external layers of epoxy resin.

Figure 10: Validation of the puzzle-like fit. A-) A miniature of the phantom head was produced to evaluate the puzzle-like fit. B) The life-size part was printed to check the geometry and test the fit between the lid and the hollow part.

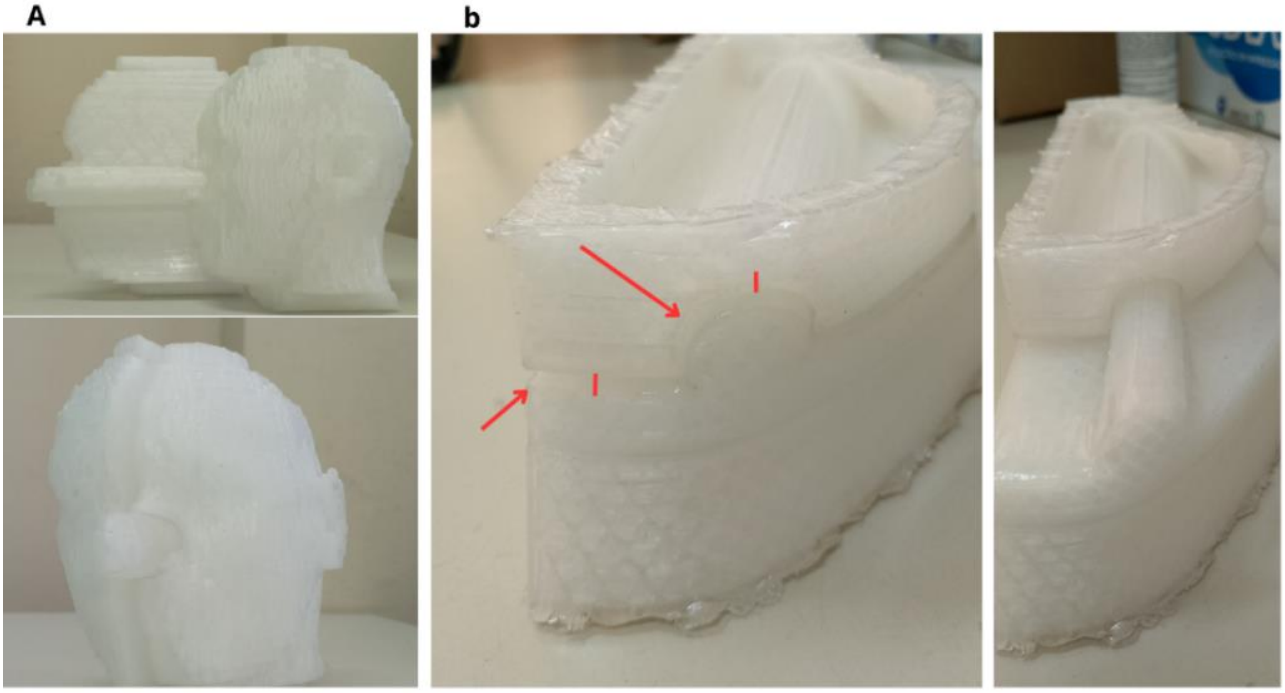

Source: Author's collection.

The first method, using pins fitting in the lid and in the hollow part, resulted in void spaces within the primary lid and the hollow part. Thus, this method was considered inappropriate to fit these pieces together. **Figure 11** illustrates the result of the second method of internal fitting of the primary lid. It is a feature that adds safety when filling the

part with radioactive material, preventing leakage. As the final result of the manipulation, a lid was obtained that allowed for the internal sealing of the phantom.

Figure 11: Result of the internal fitting. A) Note the step's presence on the lid's inside edge, which fits into the hollow part. B) The groove was obtained by subtracting the step from the 7mm edge of the hollow part.

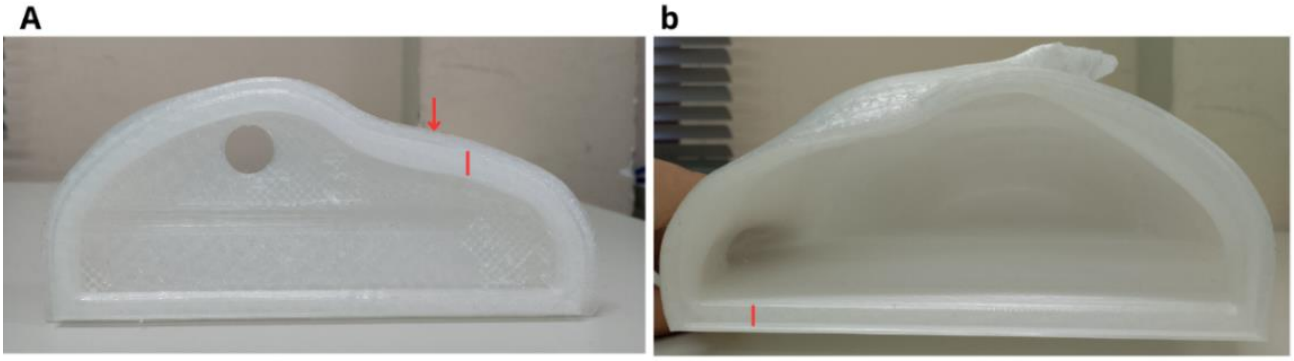

Source: Author's collection.

The new methodology of inserting puzzle-like fittings between the parts in the RMPID allowed for better assembly of the phantom and its subsequent better positioning in the WBC, eliminating the need for any other apparatus for this. In addition, the safety of the lid and hollow part fittings was improved, ensuring that the newly designed parts facilitate more efficient sealing of the phantom.

Figure 12 illustrates the RMPID full-sized printed torso painted with three layers of epoxy resin mixed with green pigment. **Figure 12 a and b** show the external view of the fitting parts and **Figure 12 c and d** the internal view of one the pieces. The green pigment makes it possible to see that the entire piece has been properly painted, avoiding possible infiltration points. Leakage tests proved the technique's effectiveness, with no leaks or infiltrations identified.

Figure 12: Full-size RMPID torso. A) External frontal view; B) External lateral view; C) Internal view of the hollow part; and D) Internal view of the lid.

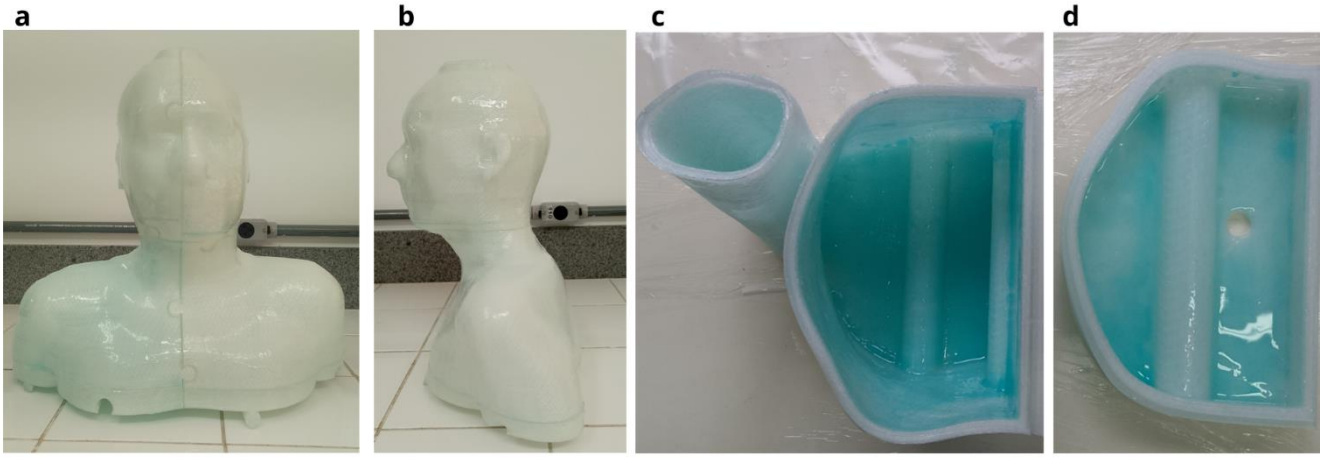

Source: Author's collection.

The next step is to complete the 3D printing of the RMPID model. Subsequently, the phantom will be filled with tissue-equivalent material containing a known activity from a radioactive nuclide.

4. CONCLUSIONS

The anthropomorphic phantom will be entirely 3D printed, measuring 176 cm and weighing 73 kg, complying with the ICRP guidelines for the reference male. This fidelity to the standards guarantees better accuracy in the calibration of *in vivo* monitoring systems, especially for male internal contamination scenarios. The methodology developed allows for the creation of customized models adaptable to the specific needs of each monitoring service. The new physical phantom will validate simulations using the ICRP-110 reference male computational model [22] for calibrating WBC virtual systems.

All the software used to generate the RMPID can be publicly accessed via the Internet, which guarantees the reproducibility of this process by other internal dosimetry groups. In addition, a brief analysis of the financial aspects of producing the RFPID [10] indicates that

additive manufacturing creates phantoms with low costs and superior geometric precision compared to current commercial simulator models. In addition, the simulator will help reduce type B uncertainties, such as the subject's positioning related to the detector and the differences between the phantom and the male subject.

ACKNOWLEDGMENT

The following Brazilian institutions support this research project, Research Support Foundation of the State of Minas Gerais (FAPEMIG - Project APQ-03582-18), Brazilian Council for Scientific and Technological Development (CNPq) and Coordination for the Capacitation of Graduated Personnel (CAPES). This work is also part of the Brazilian Institute of Science and Technology for Nuclear Instrumentation and Applications to Industry and Health (INCT/INAIS), CNPq project 406303/2022-3.

FUNDING

The research was supported by CAPES with a master's scholarship for the Postgraduate Program in Science and Technology of Radiation, Minerals and Materials (PPG-CDTN). Research Support Foundation of the State of Minas Gerais (FAPEMIG - Project APQ-03582-18) finances the project.

CONFLICT OF INTEREST

All authors declare that they have no conflicts of interest.

REFERENCES

[1] W. Li, "Internal Dosimetry: —A Review of Progress," Jpn. J. Health Phys., vol. 53, pp. 72–99, Jan. 2018, doi: 10.5453/jhps.53.72.

[2] ICRP, Ed., "Occupational intakes of radionuclides. Part 1." Sage, 2015.

[3] F. Paquet, "Internal Dosimetry: State of the Art and Research Needed," J. Radiat. Prot. Res., vol. 47, no. 4, pp. 181–194, Dec. 2022, doi: 10.14407/jrpr.2021.00297.

[4] L. Bodin and F. Menetrier, "Treatment of radiological contamination: a review," J. Radiol. Prot., vol. 41, no. 4, p. S427, Nov. 2021, doi: 10.1088/1361-6498/ac241b.

[5] A. Giussani et al., "Eurados review of retrospective dosimetry techniques for internal exposures to ionising radiation and their applications," Radiat. Environ. Biophys., vol. 59, no. 3, pp. 357–387, 2020, doi: 10.1007/s00411-020-00845-y.

[6] IAEA, Technical recommendations for monitoring individuals for occupational intakes of radionuclides. Publications Office of the European Union, 2018. Accessed: Aug. 20, 2024. [Online]. Available: https://data.europa.eu/doi/10.2833/393101

[7] Y. C. M. Staal et al., "The importance of variations in in vitro dosimetry to support risk assessment of inhaled toxicants," ALTEX, vol. 41, no. 1, pp. 91–103, Jan. 2024, doi: 10.14573/altex.2305311.

[8] B. M. Dantas, "Bases para a Calibração de Contadores de Corpo Inteiro Utilizando Simuladores Físicos Antropomórficos," Bases Para Calibração Contadores Corpo Inteiro Util. Simuladores Físicos Antropomórficos, p. 172, 1998.

[9] ICRU, "REPORT 48 - Phantoms and Computational Models in Therapy, Diagnosis and Protection | GlobalSpec." 1992. Accessed: Jul. 08, 2024. [Online]. Available: https://standards.globalspec.com/std/446666/report-48

[10] E. M. R. D. Andrade, L. Paixão, B. M. Mendes, and Telma C Ferreira Fonseca, "RFPID: development and 3D-printing of a female physical phantom for whole-body counter," Biomed. Eng. Phys. Express, 2024, doi: 10.1088/2057-1976/ad4650.

[11] A. A. Y. Kakoi, "ANÁLISE DA METODOLOGIA DE CALIBRAÇÃO DOS DETECTORES DE NaI(Tl) DO LABORATÓRIO DE MONITORAÇÃO IN VIVO DO IPEN PELO MÉTODO DE MONTE CARLO," INSTITUTO DE PESQUISAS ENERGÉTICAS E NUCLEARES-IPEN, São Paulo, 2013. Accessed: Sep. 23, 2024. [Online]. Available:

http://pelicano.ipen.br/PosG30/TextoCompleto/Adelia%20Aparecida%20Yuka%20Kakoi_M.pdf

[12] B. Breustedt, A. Giussani, and D. Noßke, "Internal dose assessments – Concepts, models and uncertainties," Radiat. Meas., vol. 115, pp. 49–54, Aug. 2018, doi: 10.1016/j.radmeas.2018.06.013.

[13] C. M. Castellani et al., "EURADOS-IDEAS GUIDELINES (VERSION 2) FOR THE ESTIMATION OF COMMITTED DOSES FROM INCORPORATION MONITORING DATA," Radiat. Prot. Dosimetry, vol. 170, no. 1–4, pp. 17–20, Sep. 2016, doi: 10.1093/rpd/ncv457.

[14] ANSI, "American National Standard--Specifications for the bottle manikin absorption phantom," Health Phys., vol. 78, no. 3 Suppl, pp. 8–22, Mar. 2000.

[15] A. L. Lebacq, M. Bruggeman, and F. Vanhavere, "Efficiency calibration of a whole-body-counting measurement setup using a modular physical phantom," Radiat. Prot. Dosimetry, vol. 144, no. 1–4, pp. 411–414, Mar. 2011, doi: 10.1093/rpd/ncq575.

[16] C. M. Castellani et al., "IDEAS Guidelines (Version 2) for the Estimation of Committed Doses from Incorporation Monitoring Data," p. 214, 2013, doi: 10.12768/6dt6-jc23.

[17] Dayeong Hong et al., "Development of a CT imaging phantom of anthromorphic lung using fused deposition modeling 3D printing.," Medicine (Baltimore), vol. 99, no. 1, Jan. 2020, doi: 10.1097/md.0000000000018617.

[18] V. Filippou and C. Tsoumpas, "Recent advances on the development of phantoms using 3D printing for imaging with CT, MRI, PET, SPECT, and ultrasound," Med. Phys., vol. 45, no. 9, pp. e740–e760, 2018, doi: 10.1002/mp.13058.

[19] Moratelli Tayrine da Silva et al., "Use of voxelized thyroid models to develop a physical-anthropomorphic phantom for 3D printing," Braz. J. Radiat. Sci., vol. 9, no. 2C (Suppl.), Art. no. 2C (Suppl.), Aug. 2021, doi: 10.15392/bjrs.v9i2C.1673.

[20] J. Tran-Gia, S. Schlögl, and M. Lassmann, "Design and Fabrication of Kidney Phantoms for Internal Radiation Dosimetry Using 3D Printing Technology," J. Nucl. Med. Off. Publ. Soc. Nucl. Med., vol. 57, no. 12, pp. 1998–2005, Dec. 2016, doi: 10.2967/jnumed.116.178046.

[21] K. Capello, M. Tremblay, A. Schiebelbein, and N. Janzen, "3D Printed Lung Phantom for Individual Monitoring," Health Phys., vol. 126, no. 5, pp. 292–295, May 2024, doi: 10.1097/HP.0000000000001777.

[22] ICRP, 2009. Adult Reference Computational Phantoms. ICRP Publication 110. Ann. ICRP 39 (2).

[23] ICRP, 2002. Basic Anatomical and Physiological Data for Use in Radiological Protection Reference Values. ICRP Publication 89. Ann. ICRP 32 (3-4).

[24] K. F. E. Xie George Xu, "Handbook Of Anatomical Models For Radiation Dosimetry," 2009, doi: 10.1201/ebk1420059793.

[25] Rasband, W. S., "National Institutes of Health, Bethesda, Maryland, USA.," ImageJ. Accessed: Oct. 24, 2024. [Online]. Available: https://imagej.net/ij/

[26] P. Cignoni, M. Callieri, M. Corsini, M. Dellepiane, F. Ganovelli, and G. Ranzuglia, MeshLab: an Open-Source Mesh Processing Tool., vol. 1. 2008. doi: 10.2312/LocalChapterEvents/ItalChap/ItalianChapConf2008/129-136.

[27] "FreeCAD: Your own 3D parametric modeler 0.21.2." Accessed: Oct. 24, 2024. [Online]. Available: https://www.freecad.org/

[28] "Autodesk Meshmixer 3.5." Accessed: Oct. 24, 2024. [Online]. Available: https://meshmixer.com/

[29] M. Savi, M. A. B. Andrade, and M. P. A. Potiens, "Commercial filament testing for use in 3D printed phantoms," Radiat. Phys. Chem., vol. 174, p. 108906, Sep. 2020, doi: 10.1016/j.radphyschem.2020.108906.

LICENSE